The Meteoritical Society

Meteoritics & Planetary Science 56, Nr 11, 2017–2034 (2021)
doi: 10.1111/maps.13758

Meteorite terrestrial ages in Oman based on gamma spectrometry and sediment dating, focusing on the Ramlat Fasad dense collection area

Åke V. ROSÉN[1]*, Beda A. HOFMANN[1,2], Frank PREUSSER[3], Edwin GNOS[4], Urs EGGENBERGER[1], Marc SCHUMANN[5], and Sönke SZIDAT[6]

[1]Institute of Geological Sciences, University of Bern, Baltzerstrasse 1+3, Bern 3012, Switzerland
[2]Natural History Museum Bern, Bernastrasse 15, Bern 3005, Switzerland
[3]Institute of Earth and Environmental Sciences, University of Freiburg, Alberstrasse 23b, Freiburg 79104, Germany
[4]Natural History Museum of Geneva, 1, Route de Malagnou, Geneva 1208, Switzerland
[5]Institute of Physics, University of Freiburg, Hermann-Herder-Strasse 3, Freiburg 79104, Germany
[6]Department of Chemistry, Biochemistry and Pharmaceutical Sciences, University of Bern, Freiestrasse 3, Bern 3012, Switzerland
*Corresponding author. E-mail: ake.rosen@geo.unibe.ch

(Received 07 December 2020; revision accepted 05 August 2021)

Abstract–We combine the search for young meteorites in the Omani-Swiss collection (~1140 fall events collected 2001–2018) using ^{22}Na and ^{44}Ti with luminescence and ^{14}C sediment ages from the Ramlat Fasad (RaF) dense collection area (DCA) of Oman to obtain combined terrestrial ages and maximum accumulation times, and test whether the proportion of young meteorites is consistent with the models of meteorite flux and weathering. Gamma-ray spectrometry data for ^{22}Na show that two (0.17%) of the meteorites in the collection fell during the 20 yr preceding this study, consistent with the rates of meteorite accumulation. In the RaF DCA, meteorites are found on Quaternary to Neogene sediments, providing constraints for their maximum terrestrial ages. ^{44}Ti activities of the RaF 032 L6 strewn field found on deflated parts of active dunes indicate an age of 0.2–0.3 ka while dune sand optically stimulated luminescence ages constrain an upper age of 1.6 ka. Extensive sediment dating using luminescence methods in the RaF DCA area showed that all other meteorite finds were made on significantly older sediments (>10 ka). Dense accumulations of meteorites in RaF are found on blowouts of the Pliocene Marsawdad formation. Our combined results show that the proportion of meteorites with low terrestrial ages is low compared to other find areas, consistent with the previously determined high average terrestrial age Oman meteorites and significantly older than suggested by models of exponential decay. Oman meteorites may commonly have been buried within dunes and soils over extended periods, acting as a temporary protection against erosion.

INTRODUCTION

During the last two decades, Oman has grown into a major source of classified meteorites with well-documented find conditions (Al-Kathiri et al., 2005; Zurfluh et al., 2016). Among the most abundant meteorite finds in Oman, ordinary chondrites, a conspicuous property is the apparent low abundance of samples with low degrees of terrestrial weathering (W0–W1). Terrestrial age dating using ^{14}C suggests that the Omani meteorite population on average is older than the hot desert meteorite populations in the adjoining United Arab Emirates and Saudi Arabia (Hezel et al., 2011; Hofmann et al., 2018; Zurfluh et al., 2016). However, the ^{14}C method cannot resolve the relative age distribution in the youngest samples, so it has so far been unclear to what extent the least weathered chondrites from Oman represent relatively recent falls and whether the proportion of relatively recent falls within the whole population is consistent with their terrestrial age distribution. Prior studies using gamma-ray spectrometry have identified two meteorites from Oman, SaU 424 (Weber et al., 2017) and SaU 606 (Rosén et al., 2020), that fell during the two decades covered by ^{22}Na

measurements of these studies (~1986–2018). In the present study, we continue the search for chondrites with young terrestrial ages among the least weathered meteorites in the Omani-Swiss meteorite search collection using the previously successful method of estimating terrestrial ages by measuring $^{22}Na/^{26}Al$ activity ratios in samples which were so far not analyzed. Furthermore, recent results showing relatively constant $^{44}Ti/^{26}Al$ activity ratios in observed chondrite falls present an opportunity to extend the low range terrestrial age estimates (approximately 20–300 a) of suitable meteorites from the collection (Rosén et al., 2020).

The current study aims to detect all recent meteorite falls among the meteorites collected during the Omani-Swiss search campaigns up to 2018 in all areas of Oman and to provide a temporal framework for the Ramlat Fasad high-density collection area at the border of the Rub' al-Khali sand desert in the southwest of Oman. Here, we attempt to bracket meteorite terrestrial ages using short-lived cosmogenic nuclides in meteorites and luminescent ages of sediments. The Ramlat Fasad area is a key area for understanding meteorite accumulation processes. Since the initiation of the Omani-Swiss meteorite collection campaigns in 2001, searches have been concentrated to the vast open plains between the Rub'al-Khali sand desert and the Arabian Sea where the desert surface is dominated by regolith soils formed on limestones of Miocene–Eocene age where typical find densities of meteorites are 0.5–2/km^2. A search conducted in 2012 in the Saudi part of the Rub' al-Khali, however, surprisingly revealed high meteorite densities (135/km^2) in small blowout areas on bedrocks of Quaternary age, in between mobile sand dunes (Hofmann et al., 2018). These findings demonstrated the potential of areas underlain by younger sediments, as is typically the case in the Rub' al-Khali basin, to host dense meteorite accumulations. Starting in 2015, we explored areas in the Rub' al-Khali in southwestern Oman (Figs. 1a and 1b), focusing on areas between the settlement of Fasad/Al Hashman (the latter is the Bedouin name) at the southern rim of the sandy desert and the Saudi border in the area of the water well "Burkana" (literally "volcano," due to its initial artesian eruption). Similar to the blowouts in the Saudi part of the Rub' al-Khali (Hofmann et al., 2018), an unusually high concentration of meteorites (32/km^2, based on 395 meteorite finds on the combined surface of 230 blowouts totaling 12.03 km^2) was subsequently found on the blowout surfaces also in this area. In total, the Ramlat Fasad area has yielded more than 500 meteorite finds so far. In order to investigate this phenomenon, by using contextual information about many meteorites recovered and temporal information about sedimentary processes in the Rub' al-Khali part of southwestern Oman, we sampled and obtained new luminescence and ^{14}C ages of representative sediments from this area. Additional sediment ages from this area are reported in a previous study (Matter et al., 2015). Together with the cosmogenic radionuclide data obtained with gamma-ray spectrometry, the luminescence ages in particular provide further constraints on the accumulation processes of meteorites in Oman.

SETTING OF THE RAMLAT FASAD AREA IN THE RUB' AL-KHALI OF SOUTHWESTERN OMAN

In contrast to the vast open plains of the Sayh al Uhaymir, Jiddat al Harasis, and Dhofar areas of Oman, where meteorites are dominantly found on regolith soils derived from Miocene limestones (Berthiaux et al., 1992; Le Métour & Platel, 1993), the Ramlat Fasad (=Fasad sandy desert) area is characterized by an association of Quaternary and probable Mio-Pliocene sediments that provide a large variation of surface types. The highest meteorite find densities were observed in blowouts close to dunes, a setting similar to that in the Saudi part of the Rub' al-Khali, about 250 km farther west (Hofmann et al., 2018). A suite of sediment luminescence ages was presented in a previous study (Matter et al., 2015) that covered both searched areas in Saudi Arabia and in Ramlat Fasad. These ages provided an initial temporal framework for the sediments on which meteorites are found.

The Ramlat Fasad area forms the southern fringe of the vast Rub' al-Khali sand desert. Apart from the dunes, which reach heights of 140 m above the plain and typically cover 60% of the area, the surface is conspicuously flat with a slight slope of 1 m km^{-1} toward the northeast (Fig. 1b) and consists of regolithic soil, with exposed bedrock in blowouts close to dunes. Due to the presence of a coastal mountain range (Qarah Mts), large wadis (ephemeral riverbeds) drain the mountains toward the Rub' al-Khali. These wadis typically show an average slope of ~1.5 m km^{-1}. At the rim of the sand desert, the wadis disappear in a complex system of ephemeral pools in between the dunes. A similar system of wadis drains the Oman Mountains in the direction of the desert, while the area in between is absent of surficial drainage (Fig. 1a).

Figure 2 shows a schematic section through the prominent sediment types in the Ramlat Fasad area. Based on Berthiaux et al. (1992), Matter et al. (2015), and our field observations, the following sediment types can be distinguished in order of decreasing age. (1) Limestones of the Eocene Dammam formation, forming outcrops of limestone pebbles rich in cherts. (2) The Marsawdad formation, of supposed Mio-Pliocene age (Berthiaux et al., 1992), consisting of sandstones with

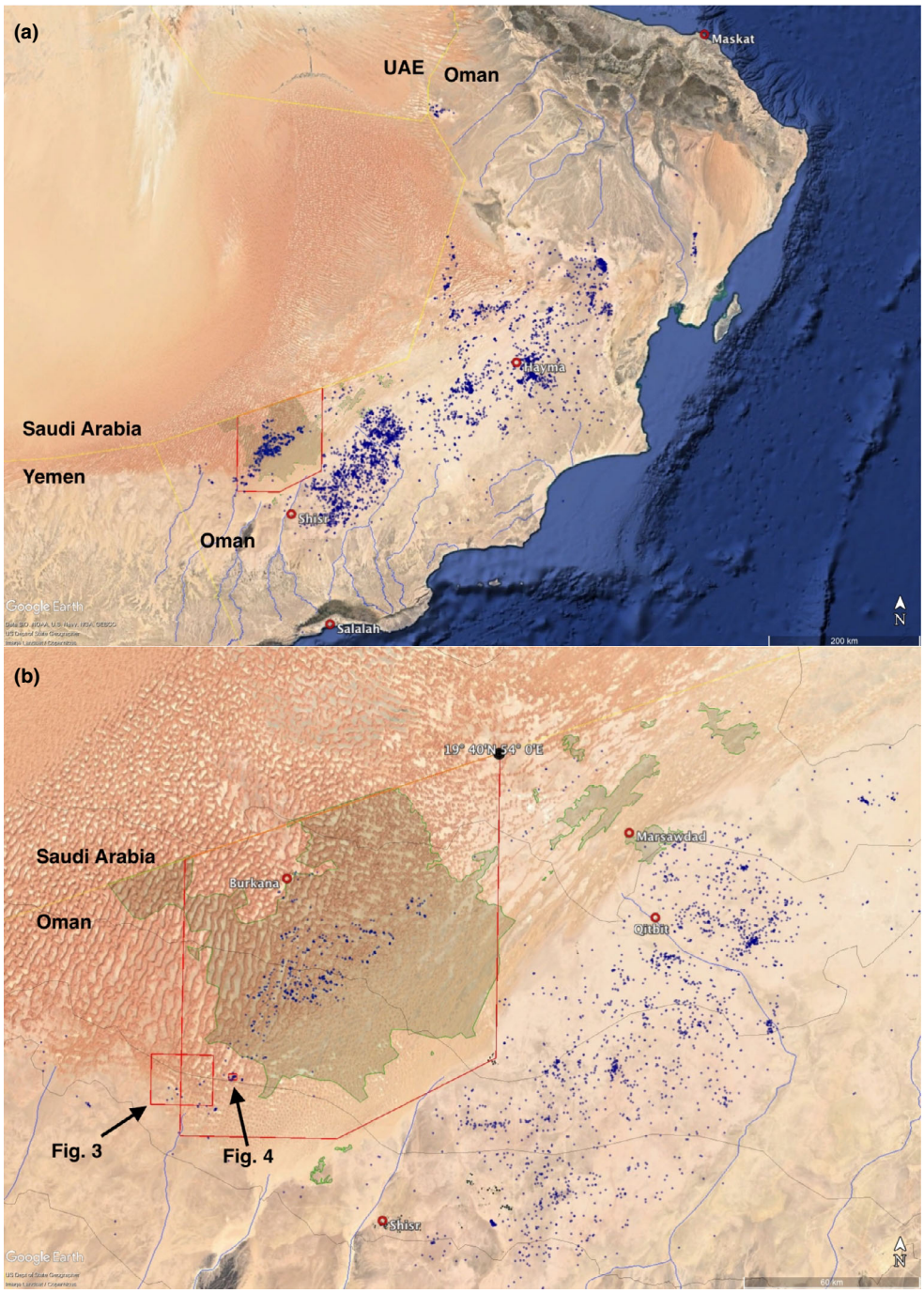

Fig. 1. Overview of meteorite finds in Oman and locations of samples. a) All meteorite finds of Oman from the Meteoritical Society database. Also shown are main drainage patterns and location of the Ramlat Fasad dense collection area. b) Detail of the Ramlat Fasad area at the southern fringe of Rub' al-Khali with outcrop area of the Marsawdad formation and locations of Fig. 3 (UaH 006) and Fig. 4 (RaF 032 strewn field). Images: Google Earth.

mixed quartz and carbonate grains, commonly showing large-scale cross-bedding that are characteristic of aeolian deposits. A few thin (<20 cm) limestone beds, free of macrofossils, are present near the top of the Marswadad formation. This formation forms the "bedrock" desert surface over an area of approximately 7000 km^2 in the Oman part of the Rub' al-Khali (Fig. 1b). (3) Deposits consisting of layered gypsum

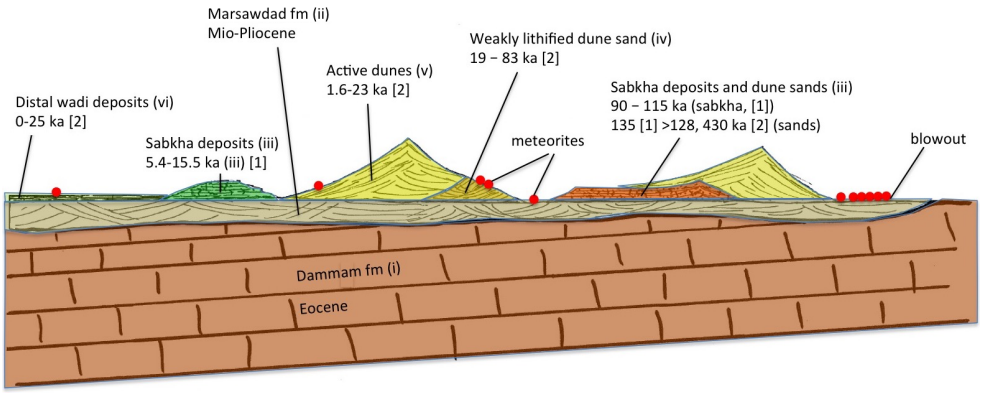

Fig. 2. Schematic cross section through prominent sediments in Ramlat Fasad.

sand, commonly exhibiting mineralized root structures that are interpreted as sabkha deposits. These are sometimes transitional to lithified dune sands, with burrows and root structures in the core of active dunes, that are morphologically placed above the peneplain surface of the Marsawdad formation. Based on prior luminescence dating (Matter et al., 2015), these scattered sabkha deposits (evaporite flats) are partly of Holocene age and in part around 100 ka old, which indicates several periods of increased humidity. (4) Weakly lithified dune sands, without root remains, that are often present in the cores of active dunes or exposed on deflated surfaces of active dunes, that is, forming a positive relief above the peneplained Marsawdad formation. (5) Active mobile (uncemented) sand dunes, recurrently developed as star dunes. (6) Distal recent wadi deposits consisting of white clays deposited from wadi-fed natural ponds in between dunes. These light-colored deposits are common in the southernmost part of the Omani Rub' al-Khali (area 18°25′ to 18°50′N and 52°30′E to 53°45′E). Coarse materials including pebbles and quartz geodes (some of them floating on water due to large voids) occur in the same area and are likely remnants of older wadi deposits formed at higher energy levels. The wadi clays are commonly interlayered with wind-blown sand. Most of the sediment material appears to have been derived from the southern coastal range (Dhofar or Qara Mts) and contains near-white clays (rich in palygorskite), which are prominent in atellite images (Fig. 3). In some cases, such clay deposits were observed to lap on active dunes, indicating temporary water depths reaching several meters. Deposits of this type apparently formed as recently as 2018, during two storm events in July and November, when major temporal lakes formed (Hansen, 2018). Recurrently, these deposits contain human debris, such as metal cans, that further attest to the recent deposition of the youngest sediments.

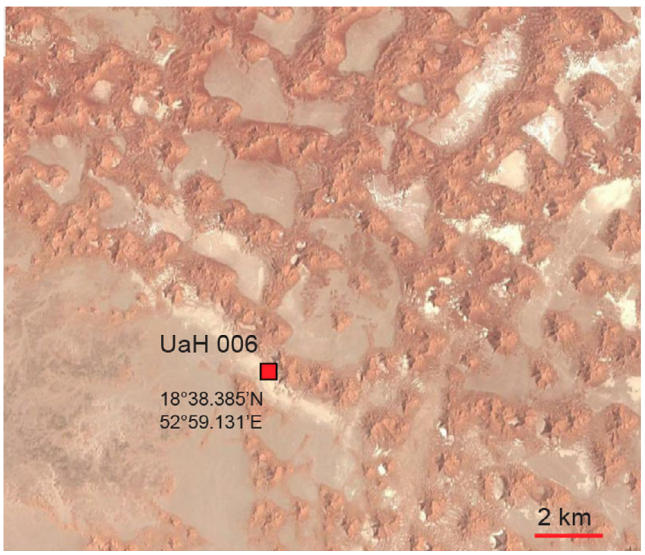

Fig. 3. Area overview (Rub' al-Khali) from where UaH 006 was found. The find location, coinciding with the area where sediment samples were collected, is marked with coordinates. Note white surfaces at the find location and in the surrounding area, which correspond to wadi flood type sediments. Google Earth image.

SAMPLES AND METHODS

Meteorite Samples and Their Context

Table 1 lists the meteorites that were analyzed by gamma-ray spectrometry in this study along with the mass and screening time of the samples that were analyzed. The meteorites were selected from the complete Omani-Swiss meteorite search collection that had been retrieved up until 2018. The selection was based on the following criteria. (1) A low degree of weathering (W0–W1) observed in thin section, according to the conventional definitions for non-Antarctic meteorites (Al-Kathiri et al.,

Table 1. List of meteorite samples analyzed by gamma-ray spectrometry.

Samples	NMBE field name	Mass (g)	Class	Weathering grade	Screening time (days)
Uruq al Hadd 015	1502_0012	253.8	H5	W1	14
Uruq al Hadd 006	1402_0030	276.2	L5	W1	14
Al Huwaysah 017	1001_0017	414.0	L6	W1	8
Jiddat al Harasis 578	0901_0055	941.3	H6	W1	8
Ramlat as Sahmah 339	1001_0047	992.0	H3.6–6	W1	6
Ramlat al Wahibah 034	0603_0056	55.2	LL3–5	W0	7
Jiddat al Harasis 703	1102_0080	34.5	H5	W1	7
Jiddat al Harasis 691	1101_0043	20.0	H5	W1	9
Ramlat Fasad 044	1502_0043	125.9	LL6	W1	14
Ramlat Fasad 058	1702_0122	56.0	L5	W3	15
Ramlat Fasad 059	1702_0177	26.3	LL6	W1	12
Ramlat Fasad 060	1802_0121	138.5	H6	W0	38
Strewn field					
Ramlat Fasad 035	1502_0030	60.6	L6	W1	10
Ramlat Fasad 033	1502_0026	366.1	L6	W1	9
Ramlat Fasad 033 prior to concentration	1502_0026	77.7	L6	W1	4
Ramlat Fasad 033 metal concentrate	1502_0026	17.4	L6	W1	61

Sample masses are given for the time of analysis.

2005; Wlotzka, 1993). From the meteorites with weathering degree 1, the samples that showed the least degree of metal oxidation (est. <5 vol% on average or in dominant segments of the studied sections) were selected. (2) For paired meteorites, the largest possible individual masses were chosen, aiming to achieve the lowest possible bulk limits of detection for short-lived cosmogenic radionuclides. The final selection encompassed individual meteorites with masses larger than 20 g. (3) Three samples were included in the study directly after having been found in 2017 and 2018. These were selected based on macroscopic appearance and included one sample with patches of light-colored matrix, still visible where fusion crust had broken off upon fall (Ramlat Fasad [RaF] 060) and additionally two (RaF 058 and RaF 059), on which the fusion crust was complete with few obvious signs of rust or wind polishing. RaF 058 afterward turned out to be of weathering degree 3, so the results obtained from this sample are mainly included for reference. Ramlat al Wahibah 034 was analyzed in a previous study (Weber et al., 2017), but remeasured in the current study, and the new results from this sample are presented as additional reference.

Samples from the Ramlat Fasad (RaF) 032 Strewn Field

A small strewn field (named after the first find, RaF 032, 6.2 g) was discovered during the 2015 Omani-Swiss search campaign. Additional samples were collected during the following year. The recovered meteorites were classified as L6 chondrites with low degrees of weathering, generally W1 but reaching W2 in some specimens. In total, 28 meteorites were found, all individuals covered with fusion crust, which made up a total mass of 660.7 g (RaF 033: 383.3 g, 7 stones 10–100 g, 15 stones 1–10 g, 5 stones <1 g, classified specimens are RaF 032, 033, 034, 035, 039, 040, 041, 042). The strewn field has an irregular triangular shape (triangle sides of 1.6, 1.3, 1.3 km) and the recovered mass generally increases toward the east (Fig. 4a). Two of the largest paired meteorites, RaF 033 and RaF 035, were selected for gamma-ray spectrometry measurements, aiming to constrain the terrestrial age of the strewn field.

While the first meteorites from the RaF 032 strewn field were found on regolithic soil on the Marsawdad formation, detailed searching revealed several specimens on deflated surfaces of active dunes (Fig. 4b). The lack of samples on significant parts of the dunes between the larger and smaller finds suggests that additional meteorites likely remain hidden in the sand. These unusual find conditions, on active dunes, prompted the idea to obtain independent terrestrial age constraints through luminescence dating directly at the find site.

Uruq Al Hadd (UaH) 006: A Meteorite on Distal Wadi Sediments

UaH 006, found in February 2014, is to this date the only meteorite in the Omani-Swiss collection that was found on distal wadi deposits (sediment type vi in Fig. 2). The surface at the find location (Fig. 3) consists of slightly deflated clayey distal wadi sediments that are interlayered with wind-blown sand on a centimeter scale, down to a depth of 35 cm.

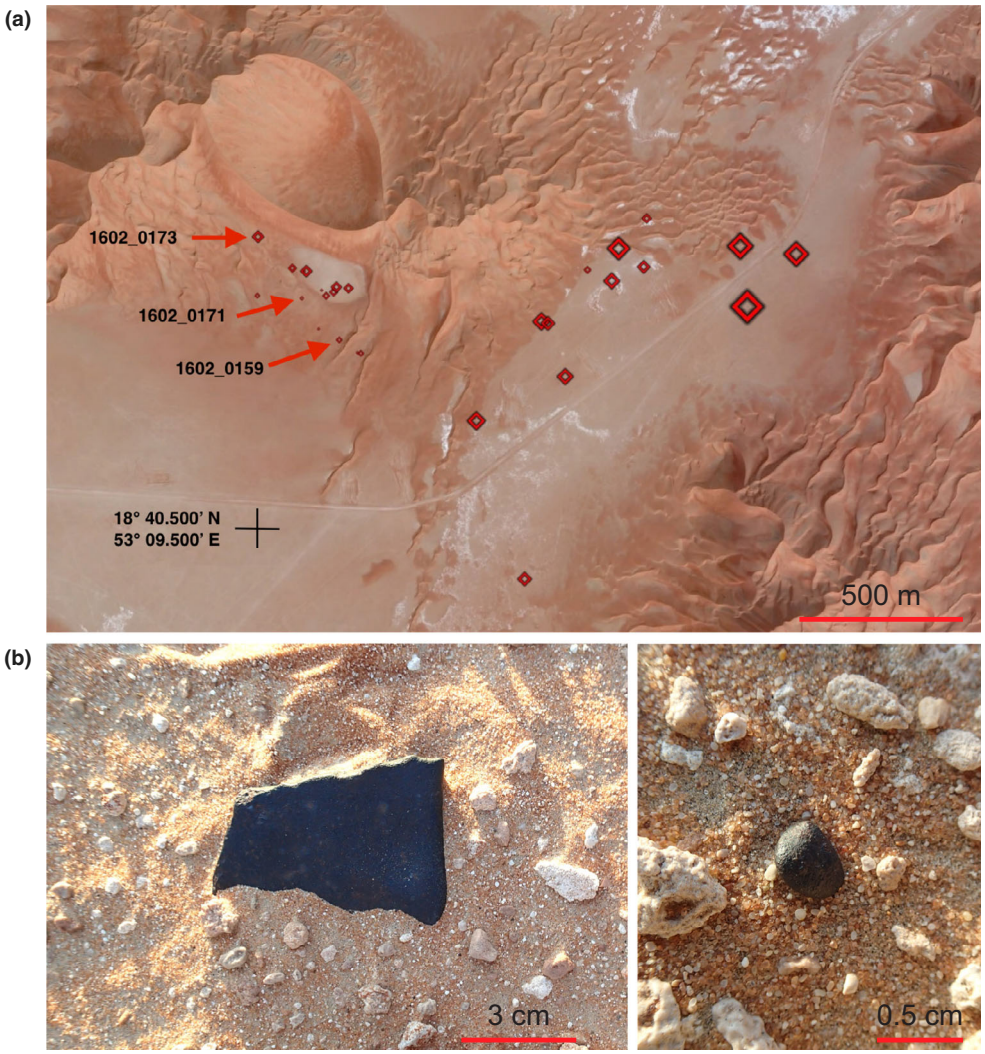

Fig. 4. The Ramlat Fasad (RaF) 032 strewn field.a) Map of the Ramlat Fasad 032 L6 strewn field showing irregular distribution of individuals with a general increase of mass toward the east. The largest symbol indicates the find location of RaF 033. Note the presence of samples on dune sands, but the higher density in deflated areas. Arrows mark three meteorite find locations on dune sand where samples for luminescence dating were collected. Symbol size indicates sample mass. Google Earth image. b) Images showing RaF 033 found on desert pavement (left) and the smallest paired sample, a complete individual of 0.175 g, as it was found on a deflated surface.

Sediment Sampling

Table 2 lists the names, descriptions, and coordinates of the sediment samples collected for luminescence dating. They were collected in the area between Fasad/Al Hashman and Burkana (artesian well at 19°16.72′N, 53°19.64′E). Samples of uncemented sand were collected at depths of approximately 30 cm beneath three exact sites where meteorites in the RaF 032 strewn field had been found on top of dunes. One sample was collected in the dark with the use of subdued red light and additionally two samples were collected using metal cylinders during the day under thick covers of blankets. Furthermore, organic fragments for ^{14}C dating were sieved from dune sand that was collected at the site. The find location of UaH 006 was revisited for sediment sampling during two search campaigns following its finding. Wadi flood-derived clay interlayered with wind-blown sand was collected at a depth of 35 cm below the exact place where the meteorite was found. The pit was dug during daylight but later enlarged and sampled during the night with subdued red light. Organic remains were separated from sediment that was sampled at 30 cm below UaH 006 after the sediment had been disaggregated in H_2O_2, mixed with water, and passed through a 1 mm sieve. Among the organic particles that were retrieved, there were wood fragments. Samples for luminescence dating of slightly lithified dune sands were

Table 2. Descriptions of the sediment samples that were collected in Ramlat Fasad at the given coordinates.

Field number	Description	Coordinates
1602-159	Dune sand 20–30 cm below meteorite	18°40.815′N, 53°9.644′E
1602-171	Dune sand 20–30 cm below meteorite	18°40.883′N, 53°9.579′E
1602-173	Dune sand 20–30 cm below meteorite	18°40.982′N, 53°9.507′E
1602-175	Weakly lithified dune sand, 30–35 cm below meteorite UaH 006	18°38.385′N, 52°59.131′E
1602-130	Sandstone, Marsawdad formation, 30–35 cm depth	19°5.648′N, 53°27.252′E
1602-131	Sandstone, Marsawdad formation, 30–35 cm depth	19°5.688′N, 53°27.061′E
1701-024	Weakly lithified dune sand, partly eroded, deeper previous burial likely (dune sand)	18°52.077′N, 53°12.211′E
1701-078	Weakly lithified dune sand, partly eroded, deeper previous burial likely (dune sand)	18°56.534′N, 53°21.071′E
1701-090	Sandstone (Marsawdad formation), partly eroded, deeper previous burial possible (dune sand)	18°56.525′N, 53°21.040′E
1702-134	Weakly lithified dune sand, deflated, deeper previous burial possible (dune sand)	18°58.335′N, 53°28.422′E
1702-366	Lithified dune sand with root remains and burrows, estimated depth below surface before bulldozing approximately 1 m	19°4.341′N, 53°20.400′E

collected using metal cylinders, hammered into the walls of pits under a thick cover of blankets. Strongly lithified sediments were collected during the night from pits dug with a hammer, using subdued red light.

Luminescence Dating

Luminescence dating was performed at the Institute of Earth and Environmental Sciences, University of Freiburg, Germany. Preparation included sieving, removal of carbonates using 10% HCl and organic material using 30% H_2O_2, as well as separation of a quartz and feldspar fraction using Na-polytungstate. The quartz fraction was etched with 44% HF (1 h, to remove remaining feldspar and the outer rim of the quartz grains) followed by 10% HCl treatment (>1 h, to dissolve fluorides). Equivalent dose (D_e) was determined using modified single aliquot regeneration (SAR) protocols for optically stimulated luminescence (OSL) of quartz (Murray & Wintle, 2000) and post-infrared (pIR) infrared stimulated luminescence (IRSL) of feldspar (pIR; Buylaert et al., 2009) using a Lexsyg Smart device (Richter et al., 2015). OSL was preheated at 230 °C for 10 s and measured at 125 °C during a 50 s exposure to blue light-emitting diodes (458 nm, 50 mW cm^{-2}), using the combination of a Hoya U-340 (2.5 mm) and a Delta-BP 365/50 EX-Interference (5 mm) filter. For pIR, samples were preheated for 60 s at 230 °C, followed by a first IRSL readout at 50 °C for 90 s and a subsequent readout at 225 °C for 100 s. Stimulation was done using IR light-emitting diodes (LEDs) with a peak emission at 880 nm (130 mW cm^{-2}), using a Schott BG-39 (3 mm) and an AHF-BrightLine HF 414/46 interference filter for detection. All samples behaved well (signal properties, performance during SAR protocol, dose recovery), and due to the presence of narrow and Gaussian-like D_e distributions, the Central Age Model (CAM; Galbraith et al., 1999) was used for the calculation of mean D_e.

Samples for dose rate measurements of approximately 500 g were dried and measured for the concentration of K, Th, and U by gamma-ray spectrometry at the Department of Chemistry and Biochemistry, University of Bern (cf. Preusser & Kasper, 2001). Alpha efficiency values were assumed at 0.07 ± 0.02 for feldspar while for quartz, the outer layer was removed during etching. Potassium content of feldspar was taken at 12.5 ± 1.0 wt % (Huntley & Baril, 1997). Water content was assumed at 4 ± 4 wt%, to allow for a wide range of environmental conditions that may have occurred at the site. Dose rate was calculated using Adele software (by D. Degering), considering longitude, latitude, and sample depth for cosmic dose rate (Prescott & Hutton, 1994).

^{14}C Dating

Organic particles which had been separated from sediments by sieving in the field and avian eggshells collected near meteorites were analyzed for ^{14}C at the Laboratory for the Analysis of Radiocarbon with AMS (LARA) at the University of Bern. The ^{14}C analysis routines are described in Szidat et al. (2014). Calendar ages were determined from the measured ^{14}C ages using the IntCal20 calibration curve with the NH Zone 1 addition (Hua et al., 2013; Reimer et al., 2020).

Meteorite Sample Preparation and Gamma-Ray Spectrometry

Radionuclides in the meteorites, listed in Table 3, were measured in the GeMSE low-background gamma-ray spectrometry facility (von Sivers et al., 2016) during 2015–2018. The listed half-lives and gamma energies are

Table 3. Analyzed isotopes with half-lives and measured energies.

Isotopes	Half-lives ($t_{1/2}$)	Gamma lines (keV)
^{26}Al	717 ka	1808.7
^{44}Ti(^{44}Sc)	60 a	1157.0
^{60}Co	5.27 a	1173.2, 1332.5
^{22}Na	2.60 a	1274.5
^{40}K	1.248 Ga	1460.8
^{137}Cs	30.08 a	661.7

from the NUDAT database (Kinsey et al., 1996). Samples were cleaned on the outside with isopropanol and each placed in a thoroughly cleaned sample bag before measurement. In order to maintain an efficient screening schedule, the sample spectra were continuously evaluated during ongoing analyses. The measurement times (Table 1) were adjusted accordingly by extending the measurements when apparent peaks from short-lived cosmogenic radionuclides were observed, as in the previously described case of SaU 606 (Rosén et al., 2020). The measurements were also extended when Bayesian statistical analysis (see von Sivers et al. [2016] for details) of the sample spectra indicated excess counts in the energy region of such gamma lines. Extra efforts were spent on samples from the RaF 032 strewn field due to the geological age constraints offered by the opportunity to date underlying sediments and the large variation of sample masses found on different types of surrounding surfaces. Metal was enriched from a cut piece of RaF 033, aiming to improve chances of detecting ^{60}Co and ^{44}Ti by concentrating the main target elements of these isotopes (Co and Fe + Ni, respectively) in a smaller mass and thereby increasing detection efficiencies while decreasing the contributions from ^{40}K and ^{26}Al to the Compton background during analyses. The starting mass amounted to approximately 78 g after trimming off rust and fusion crust. The radionuclide activities in this sample were measured prior to subjecting it to high voltage fragmentation using a SelFrag^{TM} at the Geological Institute in Bern. Suspended material was then removed and the sample left to dry at 45 °C. The remaining material was washed repeated times with ethanol and sieved into three grain fractions followed by the separation of the fractions attracted to a strong handheld magnet. These fractions were then repeatedly ground in an agate mortar, washed with ethanol, and dried after which the cycle was repeated. The obtained separate (approximately 23 g) was then leached with concentrated hydrofluoric acid for <1 h, repeatedly rinsed with deionized water, and finally rinsed with ethanol. After leaching and cleaning the material amounted to approximately 17 g. The final concentrate was wrapped in cling wrap, folded to an oblate-shaped package, and measured in the GeMSE facility during several measurement sessions amounting to a total screening time of 61 days. All counting efficiencies were simulated using GEANT4 v9.6p03 (Agostinelli et al., 2003) according to similar procedures as have previously been described elsewhere (Rosén et al., 2020; von Sivers et al., 2016). The detection efficiencies for the RaF 033 metal concentrate measurements were simulated using the bulk density given by the sample mass and measured dimensions. The chemical composition of the metal concentrate was estimated based on average L chondrite composition (Wasson & Kallemeyn, 1988) with 90 wt% of the average bulk silicate mineral fraction of typical L6 chondrites (McSween et al., 1991) deducted. The estimated 90% mass reduction of the bulk silicate fraction from the initial L chondrite starting material corresponds well to the total observed weight reduction (78%) of the starting material.

RESULTS

Luminescence- and ^{14}C Dating of Sediments Associated with Meteorite Finds

The results of OSL and pIR dating are summarized in Table 4. The IRSL ages are expected to underestimate the deposition age due to the phenomenon of fading (cf. Li et al., 2014) and are not further discussed. A comparison of OSL and pIR (Fig. 5) shows good agreement for ages below 100 ka. For three samples, pIR is significantly higher than OSL. A relative early saturation and age underestimation of quartz OSL has previously been reported from samples taken in Arabia (e.g., Rosenberg et al., 2011) and we hence interpret the older pIR ages as the more conservative ages for the three samples in question. ^{14}C data for organic particles and struthionid eggshells from the sediments are presented in Table 5.

Dune Sand Below RaF 032 Strewn Field Samples

Three samples of dune sand collected beneath the RaF 032 strewn field meteorites yielded consistent OSL and pIR ages: Samples 1602-159 (1.55 ± 0.14 ka, 1.68 ± 0.09 ka) and 1602-171 (4.87 ± 0.31 ka, 4.88 ± 0.30 ka) demonstrate a Holocene age of the sediment underlying two meteorites. For the third sample (1602-173), only an insufficient amount of feldspar could be extracted. The OSL age of 23.3 ± 1.3 ka indicates deposition during the time of last glacial maximum. Since one meteorite was collected on a deflated area with an age of approximately 1.6 ka, we take this as the maximum terrestrial age of the RaF 032 strewn field. Three samples of plant remains and a single sample of insect (ant) remains from dune sands underlying meteorites of the RaF 032 strewn field yielded recent (post-bomb) ^{14}C ages (F^{14}C 1.05–1.20, calibrated

Table 4. Results from luminescence dating of sediment samples collected in meteorite find areas in Oman. Samples (labeled) collected beneath the RaF 032 strewn field (Fig. 4) and below UaH 006 (Fig. 3) are included.

	RaF 032 Strewn field			UaH 006	Marsawdad formation			Sand deposits overlaying Marsawdad			
Field no.	1602-159	1602-171	1602-173	1602-175	1602-130	1602-131	1701-090	1701-024	1701-078	1702-134	1702-366
Depth (cm)	30	30	30	35	35	35	25	25	25	25	100
K (wt%)	0.72 ± 0.03	1.07 ± 0.04	1.12 ± 0.04	1.08 ± 0.03	0.77 ± 0.03	1.12 ± 0.04	0.37 ± 0.01	0.83 ± 0.01	0.81 ± 0.01	0.95 ± 0.01	0.80 ± 0.01
Th (μg g^{-1})	2.05 ± 0.16	1.39 ± 0.06	1.01 ± 0.06	3.38 ± 0.18	2.17 ± 0.16	3.15 ± 0.16	1.39 ± 0.07	1.10 ± 0.04	0.74 ± 0.02	1.33 ± 0.04	1.38 ± 0.04
U (μg g^{-1})	0.83 ± 0.03	0.63 ± 0.02	0.40 ± 0.02	1.34 ± 0.04	0.84 ± 0.03	1.15 ± 0.04	0.80 ± 0.03	0.49 ± 0.01	0.28 ± 0.01	0.54 ± 0.01	0.63 ± 0.01
D-Q (Gy ka^{-1})	1.19 ± 0.05	1.41 ± 0.06	1.38 ± 0.06	1.72 ± 0.06	1.25 ± 0.05	1.71 ± 0.06	0.84 ± 0.03	1.16 ± 0.04	1.06 ± 0.04	1.31 ± 0.05	1.17 ± 0.04
D-F (Gy ka^{-1})	2.01 ± 0.10	2.23 ± 0.12	n.d.	2.54 ± 0.11	1.89 ± 0.08	2.37 ± 0.10	1.30 ± 0.04	1.80 ± 0.07	1.70 ± 0.06	1.77 ± 0.06	1.63 ± 0.05
n Q/F	21/12/12	23/12/12	23/-/-	23/12/12	20/11/11	23/12/12	0/12/12	27/11/11	24/12/12	23/12/12	06/12/12
od Q/F	0.34/0.07/0.07	0.23/0.16/0.11	0.16/-/-	0.17/0.09/0.06	0.18/0.31/0.35	0.19/0.23/0.19	0.31/0.27/0.34	0.14/0.09/0.05	0.18/0.08/0.03	0.18/0.10/0.06	/0.17/0.13
D_e OSL (Gy)	1.84 ± 0.15	6.89 ± 0.34	32.21 ± 1.13	42.73 ± 1.70	151.59 ± 6.84	75.87 ± 3.20	112.76 ± 8.05	21.98 ± 0.66	29.58 ± 1.19	108.98 ± 4.15	>150
D_e IR-50 (Gy)	2.46 ± 0.05	8.04 ± 0.38	n.d.	47.11 ± 1.32	208.60 ± 19.61	86.43 ± 5.78	186.86 ± 14.64	21.39 ± 0.62	32.42 ± 0.81	115.76 ± 3.25	408.86 ± 20.84
D_e pIR-150 (Gy)	3.38 ± 0.07	10.90 ± 0.34	n.d.	63.53 ± 1.21	390.10 ± 38.23	122.16 ± 6.63	303.79 ± 29.97	30.57 ± 0.43	43.16 ± 0.50	168.61 ± 3.38	699.93 ± 27.21
Sediment ages											
Age OSL (ka)	1.55 ± 0.14	4.87 ± 0.31	23.3 ± 1.3	24.9 ± 1.3	121 ± 7	44.3 ± 2.4	135 ± 11	19.0 ± 0.9	27.8 ± 1.5	82.9 ± 4.3	>128
Age IR-50 (ka)	1.13 ± 0.07	3.60 ± 0.25	n.d.	18.5 ± 1.0	110 ± 12	36.5 ± 2.9	144 ± 12	11.9 ± 0.6	19.1 ± 0.8	65.3 ± 2.9	251 ± 15
Age pIR-150 (ka)	1.68 ± 0.09	4.88 ± 0.30	n.d.	25.0 ± 1.2	206 ± 22	51.6 ± 3.6	234 ± 24	17.0 ± 0.6	25.5 ± 1.0	95.1 ± 3.8	430 ± 27

D-Q, D-F: dose rate for quartz and feldspar, respectively; n Q/F = number of replicate measurements (OSL, IRSL, pIR); od = observed overdispersion (for OSL, IRSL, pIR).

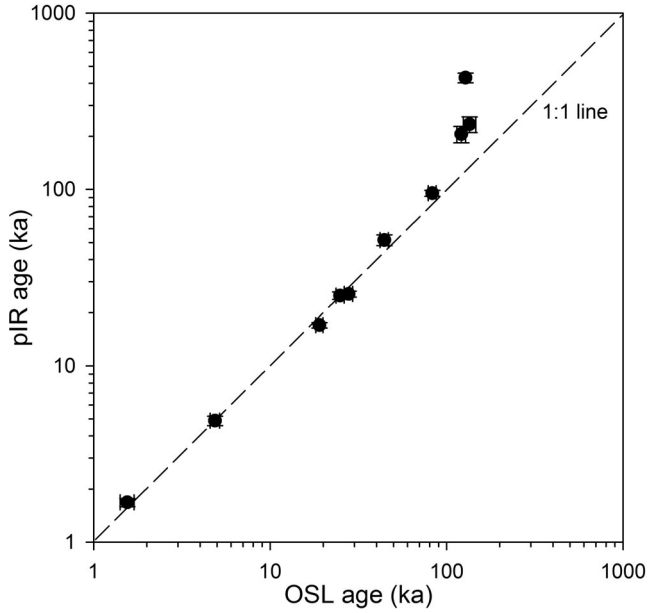

Fig. 5. Plot showing correlation of pIR ages with ages obtained by OSL. Note the very good concordance of ages up to approximately 100 ka.

ages within AD 1956–2009), indicating that the sampled organics represent recent roots and burrowing insects and are much younger than the sediment.

Wadi Flood Deposits Below UaH 006

The clayey-sandy sediments underlying UaH 006 at a depth of 35 cm yielded consistent OSL and pIR-150 ages of 24.9 ± 1.3 and 25.0 ± 1.2 ka (sample 1602-175). A small piece of wood (1402_030_org) that was taken from these sediments yielded a modern ^{14}C age ($F^{14}C$ 1.195 ± 0.07, calibrated age AD 1958–1988), suggesting sampling of a root fragment. Two other samples of clearly detrital wood fragments from the top of similar sediments in the same area yielded uncalibrated ^{14}C ages of 301 ± 18 BP (calibrated age AD 1513–1647) and 908 ± 19 BP (calibrated age AD 1045-1213).

Slightly to Strongly Lithified Dune Sands in the Core of Active Dunes

Three samples of weakly lithified dune sands on deflated surfaces of dunes, collected at the exact place of meteorite finds (Table 4), yielded consistent OSL and pIR-150 ages of approximately 17, 26, and 95 ka. The highest age is also consistent with a ^{14}C age of >48 ka for an eggshell, probably of modern ostrich (*Struthio camelus syriacus*) from the same location. Four other samples of eggshells from the slopes of active dunes and a complete ostrich egg found on regolithic soils show ages ranging from a few hundred years to >53.2 ka (on dune slope). Sample 1702-366 is lithified dune sand with burrows and root marks and yielded ages of >128 ka (OSL) and 430 ± 27 ka (pIR-150).

Marsawdad formation: Two samples from relatively strongly lithified sediments taken from blowouts in the Marsawdad formation yielded sediment ages (OSL/pIR-150) of 121 ± 7/206 ± 22 ka (1602-130) and 135 ± 11/234 ± 24 ka while sample 1702-90 yielded similar OSL and pIR-150 ages of 44 ± 2.4 and 51.6 ± 3.6 ka. Two samples of thick (2.6–3.0 mm) avian eggshells collected on the Marsawdad formation do not contain detectable ^{14}C (>48.8 and >50.2 ka).

Radionuclide Activities in the Least Weathered Fraction of Meteorites in the Omani-Swiss Collection

The gamma-ray spectrometry results are listed in Table 6 and are presented as activities at the time of measurement end for all selected meteorite samples. Activity ratios, $^{22}Na/^{26}Al$ and $^{44}Ti/^{26}Al$, or their upper limits are given separately together with determined Bayes factors for positive detections of the daughter isotope of ^{44}Ti, ^{44}Sc. Bulk ^{26}Al was 30–70 dpm kg^{-1} in all meteorites. Terrestrial contamination by ^{137}Cs was detected in all meteorites at activities below 3 dpm kg^{-1} apart from RaF 035, RaF 044, and RaF 059 from which only upper activity limits below 1 dpm kg^{-1} were obtained. The determined activities of ^{40}K correspond to K concentrations of 600–900 ppm in all bulk samples apart from RaF 058, which gave approximately 2000 dpm kg^{-1} ^{40}K, corresponding to approximately 1100 ppm K. The short-lived cosmogenic isotopes ^{22}Na ($t_{1/2}$ = 2.6 a) and ^{60}Co ($t_{1/2}$ = 5.3 a) were not detected in any of the studied samples. More long-lived ^{44}Ti ($t_{1/2}$ = 60 a) was verified in RaF 060 and the metal concentrate from RaF 033 by Bayesian statistical analyses (positive evidence for a signal at the 1157 keV main peak of ^{44}Sc).

DISCUSSION

Sediment Ages

Luminescence ages for dune sands from the RaF 032 strewn field yielded an upper age limit of approximately 1.6 ka for the fall of this strewn field and demonstrate that the different parts of a single dune vary significantly in age, from approximately 1.6 to 23 ka. The sample of distal wadi sediments 35 cm below UaH 006 was deposited approximately 25 ka ago. Considering the fact that deposition of similar sediments did occur in the area in 2018, and the presence of human debris and detrital wood just a few 100 yr old in the top of similar sediments, the sedimentation rate appears relatively low at this specific site. Attempts to obtain sediment ages by

Table 5. ^{14}C data for organic particles and avian eggshells gathered from sediments sampled in meteorite collection areas in southwest Oman.

Sample	Coordinates	Lab Code	$F^{14}C$	$\pm F^{14}C$	^{14}C age (BP)	Calendar age (95%)	Sediment type	Sample type	Shell thickness
Organic carbon									
1402-030_org	18°38.385'N 52°59.131'E	3653.1.1	1.1950	0.0067	−1431 ± 45	AD 1958–1988	Distal wadi deposits below UaH 006 (vi)	Plant remains	
1502-053_B1	18°38.550'N 53°8.750'E	3654.1.1	0.9632	0.0022	301 ± 18	AD 1513–1647	Distal wadi deposits (vi)	Plant remains (wood)	
1402_F1	18°31.950'N 53°3.100'E	3655.1.1	0.8932	0.0021	908 ± 19	AD 1045–1213	Distal wadi deposits (vi)	Plant remains (wood)	
1602_0170A	18°40.883'N 53°9.579'E	5956.1.1	1.0993	0.0045	−760 ± 33	AD 1957–2001	Mobile dune sand below meteorite (v)	Plant remains	
1602_0172 A	18°40.982'N 53°9.507'E	5957.1.1	1.2136	0.0042	−1555 ± 28	AD 1959–1986	Mobile dune sand below meteorite (v)	Plant remains	
1602_0172 B	18°40.982'N 53°9.507'E	5958.1.1	1.0563	0.0041	−440 ± 31	AD 1956–2009	Mobile dune sand below meteorite (v)	Plant remains	
1602_0172 C	18°40.982'N 53°9.507'E	5959.1.1	1.1692	0.0042	−1256 ± 29	AD 1958–1991	Mobile dune sand below meteorite (v)	Insect remains (ants)	
Egg shells									
OES3_2015	18°45.296'N 52°47.815'E	5962.1.1	0.9488	0.0037	422 ± 31	AD 1426–1618	Deflated regolith on Eocene (i)	Complete ostrich egg[a]	-
OES4_2016	19°0.530'N 53°21.991'E	5963.1.1	0.9343	0.0036	545 ± 31	AD 1321–1436	Slope of active dune (v)	Ostrich eggshell[a]	1.7 mm
1701_0004	18°45.097'N 53°11.260'E	6940.1.1	0.0011	0.0009	>46900		Sabkha sediments with gypsum (iii)	Ostrich eggshell[a]	1.6 mm
1702_0055	18°55.183'N 53°21.216'E	6941.1.1	<0.0002	0.0009	>50200		Blowout, Marsawdad formation (ii)	Struthionid eggshell[b]	3.0 mm
1702_0131	18°58.151'N 53°28.426'E	6942.1.1	<0.0005	0.0009	>48800		Blowout, Marsawdad formation (ii)	Struthionid eggshell[b]	2.6 mm
1702_0138	18°58.406'N 53°28.394'E	6943.1.1	<0.0008	0.0009	>48000		Deflated dune slope, slightly lithified (iv)	Ostrich eggshell[a]	1.5 mm
19_0152	19°13.677'N 53°34.338'E	11189.1.1	0.6690	0.0022	3229 ± 27		At base of deflated mobile dune (v)	Ostrich eggshell[a]	1.6 mm
19_0161	19°10.835'N 53°31.481'E	11190.1.1	0.9435	0.0030	467 ± 25		At base of deflated mobile dune (v)	Ostrich eggshell[a]	1.8 mm
19_0210	19°21.201'N 53°50.093'E	11191.1.1	<−0.0013	0.0007	>53200		At base of deflated mobile dune (v)	Ostrich eggshell[a]	1.6 mm

Calendar ages were determined from the measured ^{14}C ages using the IntCal20 calibration curve with the NH Zone 1 addition (Hua et al., 2013; Reimer et al., 2020) and represent 95% probabilities.

Roman numbers refer to sediment types discussed in text.

[a]Corresponds to *Struthio camelus syriacus*.

[b]Thick struthionid eggshells, *Struthio kakesiensis*?

Table 6. Radionuclide activities and activity ratios measured in meteorites from Oman (dpm kg^{-1} at finished measurement). Uncertainties of detection efficiencies were 5% for samples and 1.5% for activity ratios. Maximum activity limits are given at the 95% credible interval. Activity ratios and detected activities are given at 68%. Bayes factors (BF) correspond to evidence for positive detection of ^{44}Sc.

	Activity data								
Meteorites	^{26}Al	^{44}Ti (^{44}Sc)	^{60}Co	^{22}Na	^{40}K	^{137}Cs	($^{22}Na/^{26}Al$) $\times 10^{-2}$	($^{44}Ti/^{26}Al$) $\times 10^{-2}$	BF (^{44}Sc)
Uruq al Hadd 015	$45.6^{+2.8}_{-2.0}$	<0.59	<0.26	<0.61	1163^{+63}_{-51}	$1.14^{+0.15}_{-0.13}$	<0.85	<0.77	7×10^{-1}
Uruq al Hadd 006	$31.1^{+1.6}_{-1.7}$	<0.58	<0.27	<0.28	1514^{+67}_{-78}	$1.17^{+0.15}_{-0.16}$	<0.40	<1.01	6×10^{-1}
Al Huwaysah 017	$60.6^{+3.9}_{-2.5}$	<0.31	<0.16	<0.56	1623^{+88}_{-76}	$0.38^{+0.19}_{-0.15}$	<0.48	<0.21	2×10^{-1}
Jiddat al Harasis 578	$38.6^{+2.2}_{-1.9}$	<0.46	<0.29	<0.36	1211^{+75}_{-45}	$0.53^{+0.14}_{-0.11}$	<0.49	<0.67	5×10^{-1}
Ramlat as Sahmah 339	$49.8^{+3.0}_{-2.4}$	<0.29	<0.15	<0.55	1403^{+82}_{-59}	$0.52^{+0.17}_{-0.13}$	<0.63	<0.25	2×10^{-1}
Ramlat al Wahibah 034	$63.3^{+4.8}_{-3.2}$	<1.22	<0.69	<0.85	1392^{+82}_{-67}	$2.46^{+0.48}_{-0.45}$	<0.58	<0.89	2×10^{-1}
Jiddat al Harasis 703	$39.5^{+4.3}_{-2.0}$	<2.05	<0.48	<0.94	1195^{+78}_{-57}	$2.43^{+0.64}_{-0.39}$	<0.99	<2.77	7×10^{-1}
Jiddat al Harasis 691	$49.0^{+4.3}_{-3.5}$	<2.40	<0.48	<0.75	1311^{+89}_{-59}	$2.10^{+0.60}_{-0.57}$	<0.60	<2.59	3×10^{-1}
Ramlat Fasad 044	$43.3^{+2.6}_{-2.2}$	<0.50	<0.20	<0.56	1406^{+71}_{-74}	<0.49	<0.65	<0.54	2×10^{-1}
Ramlat Fasad 058	$64.3^{+4.4}_{-3.1}$	<0.80	<0.68	<0.97	2089^{+144}_{-76}	$1.32^{+0.31}_{-0.31}$	<0.75	<0.55	2×10^{-1}
Ramlat Fasad 059	$45.4^{+3.8}_{-2.9}$	<2.1	<0.90	<1.59	1527^{+100}_{-67}	<1.14	<1.86	<2.62	7×10^{-1}
Ramlat Fasad 060	$33.8^{+2.2}_{-1.4}$	$0.42^{+0.22}_{-0.15}$	<0.20	<0.30	1377^{+65}_{-77}	$1.34^{+0.14}_{-0.12}$	<0.42	$1.31^{+0.57}_{-0.51}$	9
Strewn field									
Ramlat Fasad 033	$68.8^{+3.6}_{-3.7}$	<0.34	<0.39	<0.58	1306^{+76}_{-54}	$0.59^{+0.14}_{-0.14}$	<0.48	<0.22	2×10^{-1}
Ramlat Fasad 035	$62.4^{+4.4}_{-3.0}$	<0.53	<0.41	<1.05	1456^{+106}_{-49}	<0.64	<0.86	<0.34	1×10^{-1}
Ramlat Fasad 033 slice	$66.8^{+5.2}_{-3.7}$	<1.17	<0.48	n.d.	1291^{+76}_{-65}	<0.64	n.d.	<1.73	3×10^{-1}
Ramlat Fasad 033 metal conc.	$56.3^{+3.2}_{-3.0}$	$0.56^{+0.35}_{-0.23}$	<0.16	n.d.	795^{+39}_{-42}	<0.12	n.d.	$1.10^{+0.51}_{-0.52}$	3

n.d. = not determined.

^{14}C dating of organic detritus in the desert sediments were generally not successful. Apparently, the analyzed particles mostly represent later contaminations that were introduced by burrowing insects or the rooting of locally grown plants. The results from ^{14}C dating do, however, confirm a recent age for the uppermost deposits of the clayey wadi flood deposit type in this part of the Rub' al-Khali.

Three samples of weakly lithified dune sands on deflated surfaces of dunes, collected at the exact place of meteorite finds, yielded consistent OSL and pIR-150 ages of approximately 17, 26, and 95 ka. The highest age is also consistent with a ^{14}C age of an avian eggshell from the same location of >50 ka. These data provide a temporal frame for the accumulation time of meteorites on the studied surfaces and are consistent with arid conditions having prevailed. The relatively high age of these inner parts of dunes also demonstrates that meteorites found on nearby blowouts on Marsawdad formation sediments may have been "stored" in the dunes over prolonged periods of time.

Sample 1702-366 represents lithified dune sand overlaying the peneplained Marsawdad formation, with abundant burrows and root marks. The sample is from the same outcrop as sample 18.4 in Matter et al. (2015), dated at 134 ± 14 ka (OSL) and 136 ± 16 ka (TT-OSL). The outcrop had been enlarged since and the newer sample was taken from a somewhat greater depth. Our new ages of >128 ka (OSL) and 430 ± 27 ka (pIR-150) indicate a complex history of this old dune core and demonstrate that the peneplanation of the Marsawdad formation is clearly older than 128–135 ka.

Three samples were taken from relatively strongly lithified sediments of the Marsawdad formation (1602-130, 1602-131, 1702-90). Sample 1602-131 yielded similar OSL and pIR-150 ages of 44 ± 2.4 and 51.6 ± 3.6 ka. We suspect that we actually sampled a pocket of more recent lithified dune sand here. The other two samples showed pIR-150 ages higher than OSL ages by a factor of 1.69 and 1.73, indicating the disturbance of at least the OSL signal. Based on the pIR-150 ages, the Marsawdad formation appears to have an age of 206 ± 22 to 234 ± 24 ka. This is in disagreement with the Mio-Pliocene age of the Marsawdad formation assumed by Berthiaux et al. (1992), and the common occurrence of thick-shelled (up to 3.5 mm) avian eggshells on the Marsawdad formation. Such thick-shelled eggs are not attributable to modern Arabian ostrich (*Struthio camelus syriacus*), but rather to a larger form that became extinct at least 3 Ma ago, for example, *Struthio kakesiensis* (Bibi et al., 2006) known from the

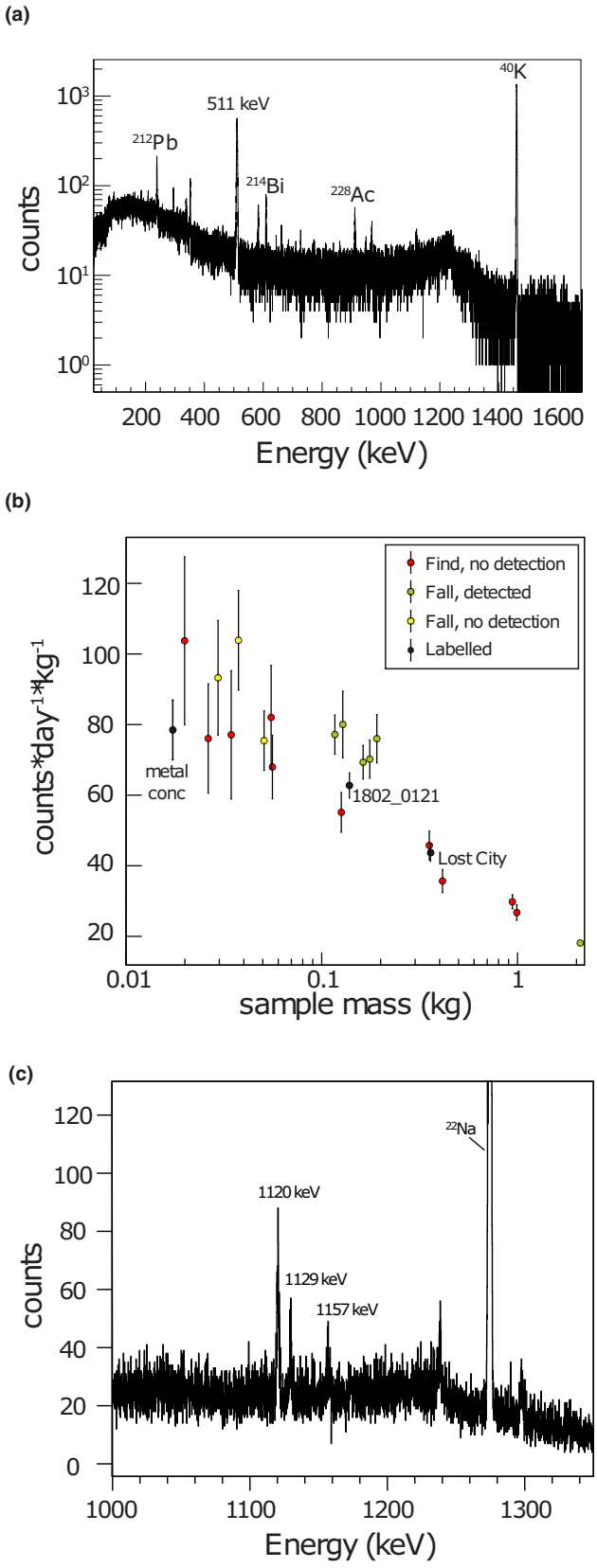

Fig. 6. a) Meteorite gamma spectrum, note the higher sample background in the low energy region. b) Plot showing sample mass versus count rate at 1157 keV $\pm 1\sigma$ divided by mass for meteorite finds (this study) and meteorite falls (Rosén et al., 2020). Falls (2008–2017) >100 g (green symbols) show higher count rate than meteorite finds (red symbols) with similar mass. Note the lower uncertainty for the largest recent fall sample (Degtevo). Recent falls (yellow symbols) and finds (red symbol) <100 g did not yield positive evidence for detection after several weeks of measurement and upper activity limits were higher than detected activities in larger sample masses from recent falls. Black symbols (labelled) show the RaF 033 metal concentrate (left), 1802_0121 (middle), and Lost City, fall 1970 (right), which yielded positive evidence for the detection of ^{44}Sc after extended screening. c) Zoom in on gamma spectrum obtained from a 2 kg mass of the recent fall (2016) Degtevo showing a clear peak at 1157 keV (^{44}Sc) and more prominent peaks. (Color figure can be viewed at wileyonlinelibrary.com.)

Arabian Emirates. With the current knowledge, we are cautious when interpreting the luminescence age data of samples with strongly different OSL and pIR-150 ages from the investigated area.

The luminescence ages provided by Matter et al. (2015) for sediments from the Ramlat Fasad area concern sabkha sediments of Holocene age (5.4–15.5 ka, no meteorite finds on these), older sabkha deposits with ages of 90–115 ka, and the fossil dune/sabkha sample from section 18.4, yielding an age of 135 ka. Figure 2 shows an overview of the different sediment types and the available ages for the area between Fasad and Burkana in the Ramlat Fasad area.

Activities of ^{44}Ti in Oman Meteorite Finds Compared to Recent Falls

The analytical approach in which the activity of ^{44}Ti in meteorites is determined by measuring the activity of the daughter isotope ^{44}Sc was established in the late 1980s (Bhandari et al., 1989). This method has several advantages compared to utilizing the low energy lines from ^{44}Ti (67.9 and 78.3 keV) in meteorite samples. The detection efficiencies are higher for the 78.3 keV line than the line at 1157 keV in GeMSE. According to our simulations, however, this difference is generally not more than 20% for typical meteorite samples with masses of 50–300 g while the sample-specific backgrounds generally are more than four times higher in the region of the ^{44}Ti low energy lines (Fig. 6a). Figure 6b shows the integrated count rates at 1156.2–1157.8 keV (1157 keV $\pm$ 1σ) in samples which were analyzed for the current study compared to count rates in previously analyzed samples from recent meteorite falls. Detection efficiencies are consistently higher for small sample masses, but the total detected counts from

^{44}Sc during several weeks are generally too low to resolve a signal against the sample-specific backgrounds in small sample masses (<100 g). In most cases, this makes it impossible to distinguish the activity of ^{44}Ti in meteorite falls from the activity in meteorite finds when analyzing small samples (approximately 50 g), even after several weeks of screening time. These give an upper activity limit which is higher than detected activities in meteorite falls and thus do not provide any information about the terrestrial age of the analyzed sample. Samples from meteorite falls with sizes of 100–200 g clearly show higher count rates at 1157 keV than meteorite finds in a similar size range, which is also reflected by the positive evidence given by our Bayesian statistical analysis. In older samples, the signal can be resolved after extended screening times or in larger sample masses. The main mass of Degtevo is the largest meteorite that has so far been measured in GeMSE. In the spectrum obtained from this meteorite, a peak centered at 1157 keV is clearly visible (Fig. 6c) after 2 weeks of measuring but with a lower intensity than the ^{26}Al peak at 1129.7 keV (branching ratio of 0.025) and the ^{214}Bi peak at 1120.3 keV (branching ratio of 0.151). The ^{214}Bi peak at 1155.2 keV (branching ratio of 0.0163) does not overlap with the 1157 keV line at the determined energy resolution and is not visible due to very low levels of ambient radon (von Sivers et al., 2016). The combined measurements of ^{44}Ti in meteorite falls and finds are consistent with earlier conclusions drawn, that terrestrial age constraints from ^{44}Ti in meteorites are mainly applicable to large sample masses and often require several weeks of measurement (Rosén et al., 2020).

Terrestrial Ages Based on ^{44}Ti/^{26}Al and ^{22}Na/^{26}Al in Meteorites

The average activity of ^{26}Al in the analyzed meteorites (RaF 033 and RaF 035 were treated as one sample) is 50 ± 11 dpm kg^{-1}, which is very similar to the average activity in 30 unpaired meteorites from Oman (53 ± 9 dpm kg^{-1}) measured previously by Weber et al. (2017). This shows that the pre-atmospheric sizes and sampled shielding depths of the least weathered chondrites from Oman that were selected for the current study are representative of the collected Oman meteorite population. The measurements on RaF 033 and RaF 035 yielded ^{26}Al activities within a range of 60–70 dpm kg^{-1}. According to the production rates calculated by Leya and Masarik (2009), this activity range corresponds to an L chondrite meteoroid with a radius of 25–65 cm. In the smaller range of pre-atmospheric meteorite sizes, these activities correspond to maximum shielding depths at the center while the opposite is true for larger meteoroids. Having previously shown that the target normalized ratio of ^{44}Ti/^{26}Al does not vary significantly between recent meteorite falls, with a similar range of ^{26}Al activities, we can use the obtained average of ^{44}Ti(Fe+Ni)/^{26}Al in H chondrites at the time of fall (0.055) to calculate a terrestrial age for the Oman finds in which ^{44}Ti was detected. This determined mean value has a standard deviation of approximately 20%, but these uncertainties are generally accounted for by the large uncertainties for single measurements of ^{44}Ti (Rosén et al., 2020). For meteorites that give total counts in the energy region of ^{44}Sc, which are sufficient to determine an upper activity limit below the activities measured in recent falls, we can determine a minimum age of the meteorite based on the upper activity limit. For small sample sizes, we are limited to minimum terrestrial age calculations based on the average ^{22}Na/^{26}Al activity ratio in ordinary chondrites, 1.5 in H, 1.35 in L and LL (Bhandari et al., 2002). This method is, however, restricted by the short half-life of ^{22}Na (2.6 a) and limits the minimum terrestrial age determination to approximately 20 a prior to analysis.

Terrestrial Age Constraints from Radionuclide Measurements

Terrestrial age constraints calculated for measured ^{22}Na/^{26}Al or ^{44}Ti(Fe+Ni)/^{26}Al activity ratios are listed in Table 7. These were calculated using the following equations:

$$Age_{T(44Ti)} = \ln\left(\frac{A_{44Ti(Fe+Ni)}}{A_{26Al} \times 0.055}\right) \times \frac{-1}{\lambda_{44Ti}} \quad (1)$$

$$Age_{T(22Na)} = \ln(1.5(\mathrm{H})/1.35(\mathrm{L})/1.35(\mathrm{LL})) \times \frac{-1}{\lambda_{22Na}} \quad (2)$$

where λ is the decay constant of ^{44}Ti or ^{22}Na, ($Fe + Ni$) is the average concentration of Fe + Ni in the chondrite class/sample, and $A_{26\mathrm{Al}}$ is the measured activity of ^{26}Al scaled to the production rates in H chondrites (L/H = 1.08, LL/H = 1.09).

The high uncertainty of the detected activity of ^{44}Ti in RaF 060 allows for a terrestrial age from present up to 60 yr ago. The upper limit of ^{22}Na/^{26}Al in this sample, however, allows for a possible terrestrial age range to be constrained by combining the minimum age set by the ^{22}Na/^{26}Al upper limit with the maximum ^{44}Ti/^{26}Al age within uncertainties. The combined results give a terrestrial age range for RaF 060 of 22–60 a. Previous detections of short-lived cosmogenic radionuclides in meteorite finds from Oman give terrestrial age constraints corresponding to a time of fall in 1998–2001 for SaU 424 (Weber et al., 2017) and 2012 for SaU 606 (Rosén et al., 2020).

Table 7. Calculated terrestrial ages and minimum terrestrial ages (as of 2018) of chondrites from Oman. The calculations were performed using activity ratios or upper limits determined at 68% C.I.

Bulk samples	Type of age constraint	Derived age	Determined by
Uruq al Hadd 015	Minimum	>66 a	$^{44}Ti/^{26}Al$
Uruq al Hadd 006	Minimum	>27 a	$^{44}Ti/^{26}Al$
Al Huwaysah 017	Minimum	>160 a	$^{44}Ti/^{26}Al$
Jiddat al Harasis 578	Minimum	>76 a	$^{44}Ti/^{26}Al$
Ramlat as Sahmah 339	Minimum	>161 a	$^{44}Ti/^{26}Al$
Ramlat al Wahibah 034	Minimum	>24 a	$^{44}Ti/^{26}Al$
Jiddat al Harasis 703	Minimum	>20 a	$^{22}Na/^{26}Al$
Jiddat al Harasis 691	Minimum	>22 a	$^{22}Na/^{26}Al$
Ramlat Fasad 044	Minimum	>67 a	$^{44}Ti/^{26}Al$
Ramlat Fasad 058	Minimum	>78 a	$^{44}Ti/^{26}Al$
Ramlat Fasad 059	Minimum	>18 a	$^{22}Na/^{26}Al$
Ramlat Fasad 060	Calculated age	22–60 a	$^{44}Ti/^{26}Al$ and $^{22}Na/^{26}Al$
Strewn field			
Ramlat Fasad 035	Minimum	>122 a	$^{44}Ti/^{26}Al$
Ramlat Fasad 033	Minimum	>161 a	$^{44}Ti/^{26}Al$
Ramlat Fasad 033 metal conc.	Calculated age	200–290 a	$^{44}Ti/^{26}Al$
Previous studies			
Sayh Al Uhaymir 606	Calculated age	8 a	Rosén et al. (2020)
Sayh Al Uhaymir 424	Calculated age	17–20 a	Weber et al. (2017)

RaF 032 Strewn Field

To calculate a terrestrial age based on ^{44}Ti measured in the metal concentrate that was separated from RaF 033, we first need to estimate the composition of the concentrate. However, large measurement uncertainties of the ^{44}Ti activity (approximately 50%) make precise compositional analysis of the concentrate unnecessary. The total activities (dpm) of ^{40}K and ^{26}Al in the concentrate make up $14 \pm 1\%$ and $19 \pm 1.5\%$ out of those measured in the starting material. Since ^{26}Al is not only produced in minerals containing Si, we instead assume the concentration of K to be representative and proportional to the remaining fraction of silicates that were initially present in the starting material. The small amount of additional material that was removed (approximately 3 wt%) is assumed to mainly have consisted of FeS. This leaves a concentrate consisting of close to 52 wt% silicates (corresponding to 14 wt% of the silicate fraction in the starting material), approximately 36 wt% metal, and approximately 12 wt % FeS. According to representative mineral chemical compositions in L6 chondrites (McSween et al., 1991), this amounts to a bulk Fe + Ni concentration of close to 50 wt%. Based on formula (1), the terrestrial age for the RaF 032 strewn field is 230^{+60}_{-30} a with stated uncertainties that correspond to the measurement uncertainties. This age is consistent with the age of 1.6 ka of the youngest underlying sand (see the Sediment Ages section) and the low degree of weathering (four samples each showing W1 and W2) for individual meteorites of this strewn field.

Accumulation of Meteorites in Oman

With this study, the search for recent falls among the finds of the Omani-Swiss meteorite search campaigns was continued and completed up to the search campaign of year 2018. While a previous study (Weber et al., 2017) covered five campaigns (2001–2006) with approximately 319 fall events and an estimated searched area of 420 km^2 (0.76 meteorites/km^2 after pairing), the present study extends the data set to 17 campaigns, approximately 1140 fall events, and a coverage of approximately 1390 km^2 (0.82 meteorites/km^2 after pairing). With the two youngest falls, which were identified based on ^{22}Na, and assuming a maximum detectable terrestrial age of 20 a for all samples, these data represent a fall rate of 72 per million km^2. This rate is consistent with the prediction of 80 falls (>10 g mass) based on Halliday et al. (1989). Our data additionally show that two of 1140 or 0.17% of the finds fell during the past 20 yr. The fraction of young falls among the whole population depends on the average survival time of meteorites (or the mean age of the population), so this fraction can thus be used to model the weathering rate of Oman meteorites. Importantly, this value is independent of the total area searched. In a simplified model, weathering (or more general: meteorite disintegration) can be assumed to follow an exponential function analogous to radioactive decay (e.g., Bland, 2001; Jull et al., 1993). From this assumption, meteorite accumulation was modeled using

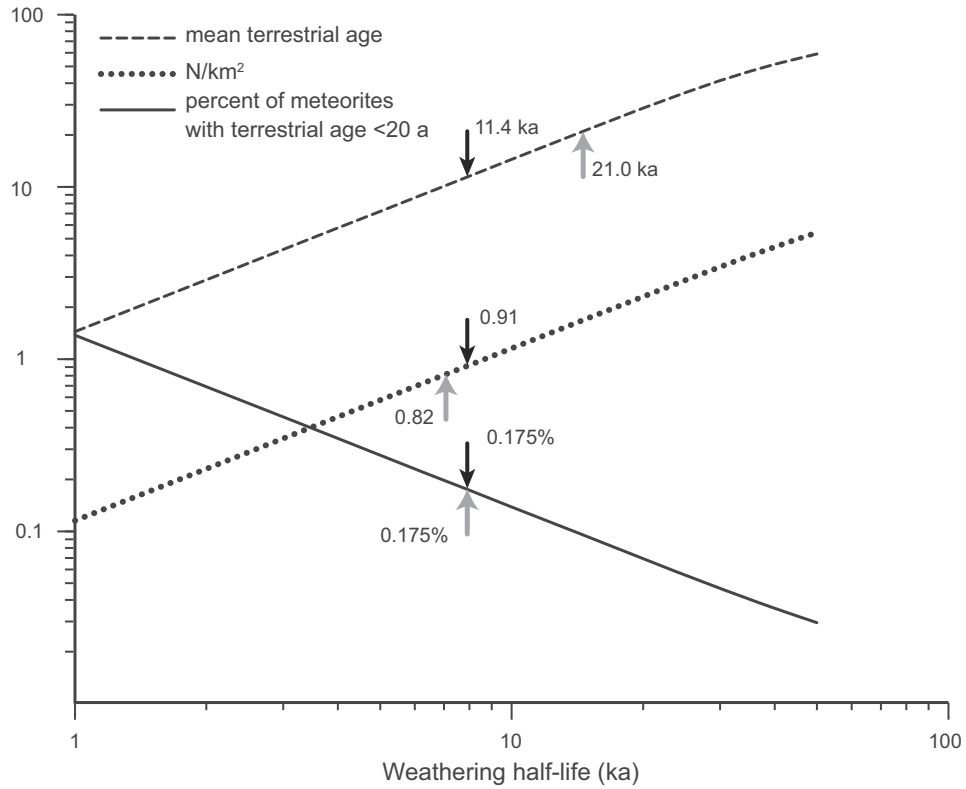

Fig. 7. Model for the accumulation of meteorites in Oman (see text). Black arrows mark modeled values for mean terrestrial age (top) and surface density (center line) for a meteorite population containing a fraction of 0.175% meteorites with fall ages younger than 20 a. Gray arrows (bottom) mark the respective observed values in the Omani-Swiss meteorite search collection of samples found in 2001–2018.

time intervals of 20 yr up to 200,000 yr, for an area of 1 km^2. For each time interval, the number of preserved meteorites was calculated from the accumulated number of meteorites using the exponential function of "radioactive decay," with half-lives varying from 1 to 50 ka. The number of preserved meteorites and age contributions were then integrated over the investigated 200,000 yr. Figure 7 shows the results from modeling the time-dependent accumulation of meteorites for an area of 1 km^2, at a rate of $80 \times a^{-1} \times 10^6$ km^2 (Halliday et al., 1989), and as a function of different "decay half-lives." The model yields (1) the percentage of young (T_t 0–20 a) meteorites among the whole population, (2) the density of accumulated meteorites, and (3) the mean age of the meteorite population. The observed fraction of 0.175% of "fresh" (T_t 0–20 a) meteorites (based on this study) corresponds to a meteorite weathering half-life of 7914 a. This half-life results in a meteorite density of 0.91/km^2 (observed: 0.82) and a mean terrestrial age of 11.4 ka (observed: 21.0 ka, $n = 128$, Zurfluh et al., 2016). While the meteorite density is consistent with our observations, the modeled mean terrestrial age is significantly lower than observed. Under real circumstances, meteorite removal is likely a non-steady process including long periods of the preservation of buried meteorites followed by rapid erosion after exhumation. This interpretation is consistent with the relatively large spread of terrestrial ages observed for chondrites with low degrees of weathering (W0–W1) combined with the relatively small proportion of such meteorites in the studied collection. Overall, both the proportion and the find density of very young (T_t 0–20 a) meteorites are consistent with the meteorite accumulation rate of Halliday et al. (1989) and correspond to a "weathering half-life" of approximately 8 ka for meteorites found in Oman.

The high density of meteorites observed in blowouts on the Marsawdad formation in the Ramlat Fasad area and the sediment ages presented in this study show that the Marsawdad formation contributes to the meteorites present in blowouts and that the dunes have slightly lithified cores with ages of commonly 20–80 ka, but extending up to several 100 ka in some cases. Meteorites found on deflated surfaces of these dunes demonstrate that meteorites can be stored (and protected from erosion) inside dunes over extended periods of time. Both the peneplained dune sands of the Marsawdad formation and the morphologically expressed dunes may act in this way.

CONCLUSIONS

The least weathered meteorites in the Omani-Swiss meteorite search collection were analyzed with the aim of identifying recent falls based on the nuclides ^{22}Na and ^{44}Ti. Combined with data from previous studies, the results show that two (or a fraction of 0.175%) of approximately 1140 sampled fall events are represented by meteorites which fell during the last two decades before this study. These numbers are consistent with the fall rate suggested by Halliday et al. (1989). According to a simplified model for meteorite accumulation and weathering, the corresponding mean terrestrial age of a meteorite in the Oman desert is 11400 a. These results combined with the significantly larger average terrestrial age determined by Zurfluh et al. (2016) suggest that meteorites in Oman commonly disintegrate in a non-steady process, involving long periods of preservation. Among the meteorites which were analyzed within the scope of the current study, one meteorite fell during 1958–1996. According to the detected activity of ^{44}Ti in a metal concentrate obtained from RaF 033, the RaF 032 strewn field has a terrestrial age of 200–300 a. This age is supported by the maximum age of 1700 a determined by luminescence dating of sediments underlying meteorites in the strewn field and ^{44}Ti/^{26}Al activity ratios in the bulk meteorites, which give a minimum age of approximately 160 a. These finds suggest that meteorites in Oman recurrently have preserved a degree of weathering corresponding to W1 during two centuries after their fall, which is consistent with the suggested disintegration process, involving stages of burial that mainly would affect meteorites in the lower range of the overall terrestrial age distribution. This is also supported by sediment age dating. To our knowledge, the Omani-Swiss meteorite collection is the only systematically searched meteorite collection in which all recent falls have been identified and their proportion determined.

Acknowledgments—This study was supported by the Swiss National Science Foundation (SNF) grant CR33I2_152941. The recovery of the meteorite samples was made in the frame of a project supported by SNF grant 200020_166251. We thank the Public Authority for Mining (Muscat, Sultanate of Oman) for supporting the Omani-Swiss meteorite search project. Open access funding provided by Universitat Bern.

Data Availability Statement—Data available on request from the authors.

Editorial Handling—Dr.A. J. Timothy Jull

REFERENCES

Agostinelli, S., Allison, J., Amako, K., Apostolakis, J., Araujo, H., Arce, P., Asai, M. et al. 2003. GEANT4—A Simulation Toolkit. *Nuclear Instruments and Methods in Physics Research Section A: Accelerators, Spectrometers, Detectors and Associated Equipment* 506: 250–303.

Al-Kathiri, A., Hofmann, B. A., Jull, A. J. T., and Gnos, E. 2005. Weathering of Meteorites from Oman: Correlation of Chemical and Mineralogical Weathering Proxies with ^{14}C Terrestrial Ages and the Influence of Soil Chemistry. *Meteoritics & Planetary Science* 40: 1215–39.

Berthiaux, A., Platel, J. P., and Roger, J.1992. *Geological Map of Shisr, 1:250'000, with Explanatory Notes*. Muscat: Ministry of Petroleum and Minerals.

Bhandari, N., Bonino, G., Callegari, E., Castagnoli, G. C., Mathew, K. J., Padia, J. T., and Queirazza, G. 1989. The Torino, H6, Meteorite Shower. *Meteoritics* 24: 29–34.

Bhandari, N., Murty, S. V. S., Shukla, P. N., Shukla, A. D., Mahajan, R. R., Sarin, M. M., Srinivasan, G. et al. 2002. Itawa Bhopji (L3–5) Chondrite Regolith Breccia: Fall, Classification, and Cosmogenic Records. *Meteoritics & Planetary Science* 37: 549–63.

Bibi, F., Shabel, A. B., Kraatz, B. P., and Stidham, T. A. 2006. New Fossil Ratite (Aves: Palaeognathae) Eggshell Discoveries from the Late Miocene Baynunah Formation of the United Arab Emirates, Arabian Peninsula. *Palaeontologia Electronica* 99: 2A.

Bland, P. A.2001. Quantification of Meteorite Infall Rates. In *Accretion of Extraterrestrial Matter Throughout Earth's History*, edited by B. Peucker-Ehrenbrink and B. Schmitz, 267–303. New York: Kluwer Academic-Plenum Press.

Buylaert, J.-P., Murray, A. S., Thomsen, K. J., and Jain, M. 2009. Testing the Potential of an Elevated Temperature IRSL Signal from K-Feldspar. *Radiation Measurements* 44: 560–5.

Galbraith, R. F., Roberts, R. G., Laslett, G. M., Yoshida, H., and Olley, J. M. 1999. Optical Dating of Single Grains of Quartz from Jinmium Rock Shelter, Northern Australia. Part I: Experimental Design and Statistical Models. *Archaeometry* 41: 339–64.

Hansen, K. 2018. Rain Soaks the Empty Corner. https://earthobservatory.nasa.gov/images/92295/rain-soaks-the-empty-quarter.

Halliday, I., Blackwell, A. T., and Griffin, A. A. 1989. The Flux of Meteorites on the Earth's Surface. *Meteoritics* 24: 173–8.

Hezel, D. C., Schlüter, J., Kallweit, H., Jull, A. T., Al Fakeer, O. Y., Al Shamsi, M., and Strekopytov, S. 2011. Meteorites from the United Arab Emirates: Description, Weathering, and Terrestrial Ages. *Meteoritics & Planetary Science* 46: 327–36.

Hofmann, B. A., Gnos, E., Jull, A. J. T., Szidat, S., Majoub, A., Al Wagdani, K., Habibullah, S. N. et al. 2018. Meteorite Reconnaissance in Saudi Arabia. *Meteoritics & Planetary Science* 53: 2372–94.

Hua, Q., Barbetti, M., and Rakowski, A. Z. 2013. Atmospheric Radiocarbon for the Period 1950–2010. *Radiocarbon* 55: 2059–72. https://doi.org/10.2458/azu_js_rc.v55i2.16177.

Huntley, D. and Baril, M. 1997. The K Content of the K-Feldspars Being Measured in Optical and Thermoluminescence Dating. *Ancient TL* 15: 11–3.

Jull, A. J. T., Donahue, D. J., Cielaszyk, E., and Wlotzka, F. 1993. Carbon-14 Terrestrial Ages and Weathering of 27

Meteorites from the Southern High Plains and Adjacent Areas (USA). *Meteoritics & Planetary Science* 28: 188–95.

Kinsey, R. R., Dunford, C. L., Tuli, J. K., and Burrows, T. W.1996. *The NUDAT/PCNUDAT Program for Nuclear Data (No. BNL-63351, CONF-961010-5)*. Upton, NY: Brookhaven National Lab.

Le Métour, J. and Platel, J. P. 1993. *Geological Map of the Sultanate of Oman. Scale 1:1.000.000*. Muscat: Directorate General of Minerals, Ministry of Petroleum and Minerals.

Leya, I. and Masarik, J. 2009. Cosmogenic Nuclides in Stony Meteorites Revisited. *Meteoritics & Planetary Science* 44: 1061–86.

Li, B., Jacobs, Z., Roberts, R. G., and Li, S. H. 2014. Review and Assessment of the Potential of Post-IR IRSL Dating Methods to Circumvent the Problem of Anomalous Fading in Feldspar Luminescence. *Geochronometria* 41: 178–201.

Matter, A., Neubert, E., Preusser, F., Rosenberg, T., and Al-Wagdani, K. 2015. Palaeo-Environmental Implications Derived from Lake and Sabkha Deposits of the Southern Rub' al-Khali, Saudi Arabia and Oman. *Quaternary International* 382: 120–31.

McSween, H. Y., Bennett, M. E., and Jarosewich, E. 1991. The Mineralogy of Ordinary Chondrites and Implications for Asteroid Spectrophotometry. *Icarus* 90: 107–16.

Murray, A. S. and Wintle, A. G. 2000. Luminescence Dating of Quartz Using an Improved Single-Aliquot Regenerative-Dose Protocol. *Radiation Measurements* 32: 57–73.

Prescott, J. and Hutton, J. T. 1994. Cosmic Ray Contributions to Dose Rates for Luminescence and ESR Dating: Large Depths and Long-Term Time Variations. *Radiation Measurements* 23: 497–500.

Preusser, F. and Kasper, H. U. 2001. Comparison of Dose Rate Determination Using High-Resolution Gamma Spectrometry and Inductively Coupled Plasma-Mass Spectrometry. *Ancient TL* 19: 19–23.

Reimer, P. J., Austin, W. E. N., Bard, E., Bayliss, A., Blackwell, P. G., Bronk Ramsey, C., Butzin, M. et al. 2020. The IntCal20 Northern Hemisphere Radiocarbon Age Calibration Curve (0–55 cal kBP). *Radiocarbon* 62: 725–57. https://doi.org/10.1017/RDC.2020.41.

Richter, D., Richter, A., and Dornich, K. 2015. Lexsyg Smart —A Luminescence Detection System for Dosimetry, Material Research and Dating Application. *Geochronometria* 42: 202–9.

Rosén, Å. V., Hofmann, B. A., Sivers, M. V., and Schumann, M. 2020. Radionuclide Activities in Recent Chondrite Falls Determined by Gamma-Ray Spectrometry: Implications for Terrestrial Age Estimates. *Meteoritics & Planetary Science* 55: 149–63.

Rosenberg, T. M., Preusser, F., and Wintle, A. G. 2011. A Comparison of Single and Multiple Aliquot TT-OSL Data Sets for Sand-Sized Quartz from the Arabian Peninsula. *Radiation Measurements* 46: 573–9.

von Sivers, M., Hofmann, B. A., Rosén, Å. V., and Schumann, M. 2016. The GeMSE Facility for Low-Background γ-Ray Spectrometry. *Journal of Instrumentation* 11: P12017.

Szidat, S., Salazar, G. A., Vogel, E., Battaglia, M., Wacker, L., Synal, H.-A., and Türler, A. 2014. 14C Analysis and Sample Preparation at the New Bern Laboratory for the Analysis of Radiocarbon with AMS (LARA). *Radiocarbon* 56: 561–6.

Wasson, J. T. and Kallemeyn, G. W. 1988. Compositions of Chondrites. *Philosophical Transactions of the Royal Society of London, Series A, Mathematical and Physical Sciences* 325: 535–44.

Weber, P., Hofmann, B. A., Tolba, T., and Vuilleumier, J. L. 2017. A Gamma-Ray Spectroscopy Survey of Omani Meteorites. *Meteoritics & Planetary Science* 52: 1017–29.

Wlotzka, F. 1993. A Weathering Scale for the Ordinary Chondrites. *Meteoritics* 28: 460.

Zurfluh, F. J., Hofmann, B. A., Gnos, E., Eggenberger, U., and Jull, A. T. 2016. Weathering of Ordinary Chondrites from Oman: Correlation of Weathering Parameters with 14C Terrestrial Ages and a Refined Weathering Scale. *Meteoritics & Planetary Science* 51: 1685–700.